

Please cite the Published Version

Joseph, Ifeoma V, Tosheva, Lubomira and Doyle, Aidan M  (2020) Simultaneous removal of Cd(II), Co(II), Cu(II), Pb(II), and Zn(II) ions from aqueous solutions via adsorption on fau-type zeolites prepared from coal fly ash. *Journal of Environmental Chemical Engineering*, 8 (4). ISSN 2213-3437

DOI: <https://doi.org/10.1016/j.jece.2020.103895>

Publisher: Elsevier BV

Version: Accepted Version

Downloaded from: <https://e-space.mmu.ac.uk/625525/>

Usage rights:  In Copyright

Additional Information: This is an Author Accepted Manuscript of a paper accepted for publication in *Journal of Environmental Chemical Engineering* published by and copyright Elsevier.

Enquiries:

If you have questions about this document, contact openresearch@mmu.ac.uk. Please include the URL of the record in e-space. If you believe that your, or a third party's rights have been compromised through this document please see our Take Down policy (available from <https://www.mmu.ac.uk/library/using-the-library/policies-and-guidelines>)

SIMULTANEOUS REMOVAL OF Cd(II), Co(II), Cu(II), Pb(II), AND Zn(II) IONS FROM AQUEOUS SOLUTIONS VIA ADSORPTION ON FAU-TYPE ZEOLITES PREPARED FROM COAL FLY ASH

Ifeoma V. Joseph*, Lubomira Tosheva, Aidan M. Doyle

Department of Natural Sciences, Manchester Metropolitan University, Chester Street, Manchester M1 5GD, United Kingdom

*Corresponding author: i.joseph@mmu.ac.uk

ABSTRACT

This study reports the potential for the simultaneous removal of Cd(II), Co(II), Cu(II), Pb(II), and Zn(II) ions from aqueous solutions by FAU-type zeolites prepared from coal fly ash. The zeolite synthesis route was via alkaline fusion followed by the addition of deionised water and hydrothermal treatment using fly ash to water mass ratios of 4, 10, 15, and 20. XRD, XRF, SEM and N₂ adsorption measurements were used to characterize the prepared zeolites. Adsorption experiments were carried out for variations in concentration, time, and adsorbent loading. The adsorption process followed pseudo second-order kinetics and Langmuir adsorption isotherm; intra particle diffusion model fitting indicated that diffusion within the pores affected the rate controlling steps and mass transfer across boundary layers for the adsorbate – adsorbent system. The efficacy of FAU – type zeolite for the quinary-metal ions adsorption studied decreased in the order Pb(II) > Cu(II) > Cd(II) > Zn(II) > Co(II).

Keywords: heavy metals; adsorption isotherm; fly ash; zeolite; pseudo second-order; coal fly ash

1. INTRODUCTION

The release, accidental or premeditated, of toxic metals to the environment as a result of industrialization continues to be a cause for global concern due to the impact on the environment and the health of living organisms [1]. For instance, trace amounts of metals like copper, iron, and zinc are essential for metabolism in all living organisms; excess amounts of these essential metals are capable

of overwhelming the homeostatic mechanism, i.e. the ability to regulate complex metabolic equilibria, of an organism [2,3]. The toxicity of cadmium, cobalt, copper, lead, and zinc vary. While some are lethal even in small concentrations, others are lethal from bioaccumulation; toxic effects range from disruption of the nervous system to carcinogenic potentials [4–6].

Adsorption is one of the effective means of the removal of these toxic metals in solutions via the use of adsorbents [5–7]. As far back as 1884, when Venable collected rudimentary data on zinc contamination [8], advances have been made in the detection, quantification, and removal of toxic metals from drinking water. Among a plethora of inorganic waste materials for purifying water contaminated with toxic metals, coal fly ash and zeolites prepared from coal fly ash have been widely used [9–14]. There is an appreciable amount of literature available on the preparation of synthetic zeolites from coal fly ash [12–18].

Coal fly ash, powdered particulate matter generated as a combustion by-product in thermal power stations that utilize pulverised coal, is mainly composed of oxides of silicon and aluminium. Pulverized coal is fed into dry bottom boilers, most commonly used in thermal power stations, and approximately 80% of all its ash is fly ash conveyed by flue gases [19]. In accordance with ASTM C618, fly ash falls into two broad classes – C and F [20]. This classification is based on the total amount of oxides of silicon, aluminium, and iron present. Class C fly ash is obtained from the combustion of geologically younger sub-bituminous or lignite coal while class F is obtained from much older bituminous or anthracite coal. According to ASTM C618 classification, the sum of SiO_2 , Al_2O_3 , and Fe_2O_3 is up to 50% for class C and 70% for class F [20]. The chemical composition of coal fly ash (CFA) varies with geographical location and the coal source but the commonality is the predominance of SiO_2 and Al_2O_3 . The phases in fly ash typically include crystalline structures like mullite, hematite, magnetite, and quartz [1,16].

Due to the close semblance in terms of composition of CFA to volcanic materials, fly ash can be used to synthesize zeolites. Zeolites are 3D aluminosilicate frameworks with porous crystalline structures that have wide ranging usage in the fields of adsorption, catalysis, and ion exchange [18,21–26]. Zeolite types from CFA include Linde type A zeolite (LTA), FAU-types (zeolite X, Y), zeolite P, and chabazite

[1,14,27–29]. To synthesize zeolites from CFA, the conventional methods involve the use of alkaline solutions to dissolve the varied crystalline phases and the subsequent precipitation of zeolite phases via hydrothermal treatment, whereas unconventional methods include dry or molten salt conversion and microwave assisted synthesis [29–32]. The hydrothermal method for CFA synthesis typically involves heating CFA in NaOH solutions at autogenous pressures using a temperature range of 80 – 200 °C and a time period of 3 to 96 h [21,29,33,34]. With the variations in alkali concentrations, solid to liquid mass ratio, type of CFA, synthesis temperature and time, the yields of zeolitic materials, including zeolite A, Na-P1, and hydroxysodalite, were reported to be between 20 – 65 wt % of CFA [33–35]. An improvement on the hydrothermal method is the inclusion of an alkaline fusion step prior to the hydrothermal treatment developed by Shigemoto et al. [36]. In this method, CFA is mixed with various mass ratios of CFA to solid NaOH and the product is fused at temperatures ranging from 400 - 750 °C; this converts most of the crystalline CFA phases into soluble aluminosilicates, which are then dissolved in distilled water and subsequently crystallized into zeolites via hydrothermal synthesis [16,33,36–39].

Polluted effluent water, with concentrations above the regulated limit, contains a myriad of metal ions and, as such, mono or bi adsorption systems are not realistic, hence the need for simultaneous multi-metals adsorption systems. This paper reports the synthesis of FAU - type zeolites from coal fly ash (CFA) via fusion - hydrothermal method and the use of the prepared zeolite for the simultaneous removal of Cu(II), Cd(II), Pb(II), Co(II), and Zn(II) in a five metals adsorption system.

2. EXPERIMENTAL

2.1 Materials

Fly ash was obtained from the Lethabo Power Station in the Free State region of South Africa. Powdered sodium hydroxide and nitrate salts of copper, lead, cobalt, cadmium, and zinc were purchased from Sigma Aldrich (99.999 % trace metal basis).

2.2 Zeolite Synthesis

Coal fly ash (CFA) was mixed with powdered NaOH at a mass ratio of 1:1.2 and the mixture was fused at 600°C for 3 h [17,37]. After fusion, fused CFA sample was ground in a mortar and a precise amount

placed in a polypropylene reactor with the addition of deionized water at a sample to water mass ratio of 1:4, 1:10, 1:15, and 1:20. The samples were aged for 24, 48, 68, and 72 h, and then transferred to an 80°C preheated oven for 24 h hydrothermal treatment at autogenous pressure. After hydrothermal treatment, the samples were filtered, washed several times to ensure the removal of excess NaOH, and dried overnight at 90°C. The samples obtained were denoted CFZ4 - n, CFZ10 - n, CFZ15 - n, and CFZ20 - n where the numbers denote precursor water content and n denotes ageing duration (24, 48, 68, and 72 h). A reference FAU zeolite (ZRef-FAU) was prepared as reported by Valtchev and Bozhilov [17,40] for comparison with the zeolites prepared from CFA.

2.3 Characterization

Crystallographic data were obtained with a Panalytical X'Pert Diffractometer (XRD) using Cu K α radiation at a scan step size of 0.013130° over a 2 θ range from 4° - 50°. Chemical analysis was performed with a Rigaku NEX-CG X-ray Fluorescence (XRF) spectrometer. Scanning Electron Microscopy (SEM) images were obtained with a Carl Zeiss Supra 40VP SEM while a semi-quantitative elemental analysis was done using an EDAX Inc. Apollo 40SDD Energy Dispersive X-ray Spectroscopy (EDAX) detector. A Micromeritics ASAP 2020 was used to measure nitrogen adsorption isotherms at -196 °C; samples were degassed at 300 °C for 3 h prior to analysis. Surface areas were calculated using the Brunauer-Emmett-Teller (BET) model and external surface areas and micropore volumes were determined by the t-plot method.

2.4 Batch Adsorption Experiments

Appropriate amounts of metal salts were used to prepare a stock solution of 1000 mg/L in each metal making a total of 5000 mg/L of 5 metals. Subsequent dilutions were made to obtain concentration ranges of 100-500 mg/L. Adsorption experiments were carried out in triplicates at room temperature with sample volume of 20 mL and an appropriate amount of adsorbent in a 120 mL polypropylene bottle under mechanical shaking using a Gerhardt Laboshake for 90 min; in the case of kinetics experiments, the duration was 0-180 min. Prior to the adsorption runs, the effect of the polypropylene bottles was checked by carrying out the experiments without the addition of adsorbent to know if the bottles

adsorbed metals. 200 mg/L initial concentration was used for optimal time and adsorbent loading tests. To determine the optimal time, aliquots of the solutions with the adsorbent (CFZ10-68) in 120 mL polypropylene bottles were taken at 10, 15, 30, 45, 60, 90, 120, 150, and 180 min. The adsorbent amount was varied for 5, 10, and 15 g/L to determine the effect of adsorbent loading. Isotherm parameters were determined at concentrations of 100, 150, 200, 250, 300, 350, 400, 450, and 500 mg/L. At the end of the adsorption experiments, the samples were centrifuged at 3800 rpm for 4 min and analysed with Thermo Scientific ICP-OES (iCAP 6000 series).

Analysis of the data obtained from ICP-OES was done for data fitting to adsorption isotherms and kinetics models. The efficiency, percentage of heavy metals removed, was obtained as shown in equation (1):

$$\text{Removal efficiency (\%)} = \left(\frac{C_i - C_f}{C_i} \right) 100 \quad (1)$$

Where C_i and C_f are the initial and final (equilibrium) concentrations respectively (mg/L).

Equation (2) shows the sorption amount, q_e , representing the amount of heavy metals adsorbed on the adsorbent.

$$q_e \text{ (mg/g)} = \frac{(C_i - C_e)}{m} V \quad (2)$$

where V is the volume of the solution in L and m is the mass of adsorbent (g), respectively, while C_e is the equilibrium concentration in mg/L.

Adsorption isotherms include Langmuir, Freundlich, and Dubinin – Radushkevich. A linear form of the Langmuir adsorption model can be written as shown in equation (3):

$$\frac{C_e}{q_e} = \frac{1}{(K_L)(q_{max})} + \frac{C_e}{q_{max}} \quad (3)$$

K_L is the Langmuir constant (L/mg) while q_{max} is the maximum metal ion adsorbed (mg/g).

Adsorption kinetics governing the sorption process determine the rate of adsorption. It is also an indicator of chemisorption (adsorption via chemical reaction between the adsorbate and adsorbent

surfaces involving valence forces) or physisorption (adsorption controlled by van der Waals Forces) [1,41]. These kinetic models include first, pseudo first, second, or pseudo second-order shown in equations (4) to (6); k_1 , k_{PFO} , k_2 , and k_{PSO} are the rate constants for first, pseudo first, second, and pseudo second-order respectively; t is the time. C_i and C_t are concentrations at the initial time and time t , while q_t and q_e are the amount of heavy metals adsorbed at time t and equilibrium respectively.

$$\text{First - order: } \ln C_t = \ln C_i - k_1 t \quad (4)$$

$$\text{Pseudo first - order (Lagergen equation): } \log(q_e - q_t) = \log(q_e) - \frac{k_{PFO}}{2.303} t \quad (5)$$

$$\text{Second - order: } \frac{1}{C_t} = \frac{1}{C_i} + k_2 t \quad (6)$$

$$\text{Pseudo second - order: } \frac{t}{q_t} = \frac{1}{k_{PSO} q_e^2} + t \left(\frac{1}{q_e} \right) \quad (7)$$

The intraparticle diffusion model, which accounts for diffusion within the pores of the adsorbents, is given by equation (8) with k_i denoting the intraparticle diffusion rate constant [42,43]:

$$q_t = k_i t^{0.5} \quad (8)$$

3. RESULTS AND DISCUSSIONS

3.1 Characterization of Coal Fly Ash (CFA)

In determining the physicochemical properties of the raw CFA, the XRD pattern, Fig. 1a, shows that CFA is mainly composed of quartz and mullites. SEM analysis, Fig. 1b, shows the characteristic spherical shape associated with CFA with a very smooth surface possibly due to the surface layer of aluminosilicate glass phase [44]. XRF results for the major oxides were SiO₂ 59.0 mass%, Al₂O₃ 37.50 mass%, CaO 4.86 mass%, Fe₂O₃ 2.61 mass%, TiO₂ 1.62 mass%, and MgO 1.30 mass%. In accordance with ASTM C618 standard, this is a class F fly ash [20]. The Si/Al molar ratio of the CFA was 2.66 (mass ratio of 1.57), and the BET surface area was 2.0 m²/g.

3.2 Zeolite Synthesis

Fig. 2 depicts the crystallographic changes that accompanied the transformation of CFA into zeolite. With alkali fusion, the Si/Al ratio was reduced to 1.52 with the dissolution of aluminosilicate phases leaving predominantly amorphous phases after ageing. Proceeding with hydrothermal treatment at 80°C, the intermediate amorphous phases reorganized and zeolite nucleation with crystal growth occurred within the treatment duration. XRD patterns show distinct crystalline features predominantly composed of FAU-type zeolite as seen in Fig.2 (CFZ10-68) with a peak by peak match in relation to the reference zeolite (ZRef-FAU).

3.2.1 Effects of Water Content and Ageing Duration

The XRD patterns of samples CFZ4 and CFZ10 with different ageing times and the reference zeolite (ZRef-FAU) are shown in Fig. 3 while the corresponding SEM images are shown in Fig. 4. With a water content of 1:4, the end product formed with 24 h of ageing was mainly a mixed phase that includes FAU (Fig. 3 and Fig. 4a). An extended ageing duration of up to 72 h resulted in a mixture of FAU and LTA zeolites (Fig. 4 a-d). A higher water content of 1:10 and 24 h ageing resulted in a more defined FAU zeolite structure (Fig 4e). As shown on Fig. 4f-h, ageing extensions for 48, 68, and 72 h resulted in clearly defined distinctive octahedral morphology of FAU-type zeolites.

All CFA zeolites had a Si/Al ratio of about 2.5, which is comparable to the Si/Al ratio of the raw CFA (Table 1). Surface areas, external surface areas and micropore volumes increased with an increase of ageing time up to 68 h for both CFZ4 and CFZ10 zeolites. Further increase of the ageing time resulted in a slight reduction of the micropore volume in both type of samples, which could be due to an increased amount of LTA-type zeolite in the samples as seen in the XRD patterns (Fig. 3). CFZ10 samples showed superior crystallinity and contained lower amount of trace phases compared to CFZ4 samples. The most crystalline sample, CFZ10-68, had a micropore volume of 0.172 cm³/g compared to 0.304 cm³/g for the reference material (Table 1), which could be due to the presence of trace materials such as LTA, which do not adsorb nitrogen.

In a series of experiments, the water content was increased even further using the optimised 68 h of ageing, in an attempt to increase the phase purity of the FAU-type zeolites. The results shown in Fig. 5

indicate that when a ratio of 15 was used, the FAU phase purity indeed increases. However, further increase of the ratio to 20 resulted in a disordered material. These results were also confirmed by the surface area and micropore volume results obtained (Table 2). XRD of the precursor samples prior to being subjected to hydrothermal treatment were very similar (Fig. 5a) indicating that minor variations in the chemical composition of the precursor mixture have a significant influence on the zeolite crystallization during the hydrothermal step. With an increment in water content from 1:4 to 1:20 ratios, within the same ageing duration of 68 h, the result showed that FAU zeolite was formed up until 1:15 (CFZ4-68, CFZ10-68, and CFZ15-68). Beyond that, the product was predominantly amorphous (CFZ20-68), as shown on the XRD patterns in Fig. 5b. As shown on Fig. 5a, for all the water additions of 1:4, 1:10, 1:15, and 1:20 (CFA4-68, CFA10-68, CFA15-68, and CFA20-68, respectively), the XRD patterns for the samples prior to hydrothermal treatment (where the samples were filtered and washed after ageing) showed that the amorphous signatures appeared the same irrespective of the amount of water added. Hydrothermal treatment re-introduced crystallinity via zeolitization making FAU the dominant phase from a water ratio of 10 to 15 (CFZ10-68 and CFZ15-68) with a subsequent increase in Si/Al ratio and surface area shown on Table 2. For the prepared zeolites, Fig. 5b shows the amorphous structure of CFZ20-68 is similar to its pre-hydrothermal treatment stage as seen on the XRD pattern of CFA20-68 (Fig.5a) with a surface area of 27 m²/g (Table 2) compared to CFZ15-68, which has a surface area of 465 m²/g.

Nitrogen adsorption/desorption isotherms of CFZ10-68, CFZ15-68, and ZRef-FAU are shown in Fig. 6a and corresponding BJH (Barrett, Joyner, and Halenda) adsorption pore-size distributions are included in Fig. 6b. The isotherm of the reference sample displays a typical type I isotherm characteristic of microporous materials. The micropore volume of this sample (0.303 cm³/g, Table 1) confirms the fully crystalline zeolite FAU nature of the sample (Fig. 2). The shape of the isotherms of CFZ10-68 and CFZ15-68 is different in comparison with the reference zeolite. The isotherms contain a hysteresis loop, however, due to the absence of a plateau at high relative pressures they can be classified as type IIb isotherms rather than type IV isotherms [45,46]. The type H3 hysteresis loops in both samples suggest the presence of slit-shaped pores. The steep increase in the volume of gas adsorbed

at low relative pressures is indicative of microporosity, and corresponding micropore volumes of 0.172 and 0.194 cm³/g, Table 2, were determined, which are lower compared to the micropore volume of the reference zeolite sample in accordance to XRD results (Fig. 3). The BJH pore-size distributions further confirm the similar pore structures of CFZ10-68 and CFZ15-68 (Fig. 3b).

3.3. Simultaneous Adsorption

3.3.1 Adsorbent tests: removal efficiency

Fig. 7 shows the use of raw fly ash, CFA, as an adsorbent in simultaneous adsorption experiments for a concentration range of 5 to 100 mg/L. At the lowest concentration of 5 mg/L, less than 65% of Co and Cd were removed while Cu and Pb had more than 98% removal. The decline in the removal efficiency followed a similar gradation for Cd and Co. Below 20 mg/L, the efficiency trend was Cu(II) > Pb(II) > Zn(II) > Co(II) > Cd(II). Above 20 mg/L, it was Pb(II) > Cu(II) > Cd(II) > Zn(II) > Co(II). With a surface area of 2 m²/g and well-defined crystalline phases (Fig. 1a) consisting of aluminosilicates albeit not in the same ordering as FAU zeolite, adsorption was possible even in the presence of a myriad of impurities in the untreated fly ash.

Transformation of CFA to FAU zeolite lead to the restructuring of the constituent crystalline phases and a major enhancement of the adsorption experiment results of the untreated fly ash; even though CFZ15-68 had the highest surface area of 465 m²/g, CFZ10-68 was used instead in consideration of a lesser amount of water for synthesis . While the quantity of adsorption on CFA was limited below 100 mg/L, FAU zeolite from fly ash (CFZ10-068) had a removal efficiency of almost 100% at 100 mg/L (Fig. 8a). A better comparison is with the reference FAU zeolite, ZRef-FAU shown in Fig. 8b. While CFZ10-68 followed a trend of Pb(II) > Cu(II) > Cd(II) > Zn(II) > Co(II), ZRef – FAU had a trend of Pb(II) > Cd(II) > Cu(II) > Zn(II) > Co(II) for an initial concentration range of 100 – 500 mg/L at 5 g/L adsorbent loading for a duration of 90 minutes. The reversing of Cd(II) and Cu(II) removal efficiencies between CFZ10-68 and ZRef-FAU could be due to the presence of amorphous material in the former as well as differing elemental compositions, for instance the presence of Fe₂O₃ and CaO (2.19 wt% and 3.45 wt%, respectively) in CFZ10-68, which were absent in the reference sample according to XRF.

Even with five metals with differing physical and chemical properties in competition for the available adsorption sites, Pb(II) consistently achieved up to 99% removal at the maximum concentration for both samples. Up to a concentration of 350 mg/L, CFZ10 – 68 could remove more than 80% and 75% of Cu(II) and Cd(II) respectively; Zn(II) was almost 40% removed and Co(II) with less than 20% reached a point beyond which removal was not feasible. As the amount of competing ions increased above 350 mg/L in the solution, any apparent selectivity for Zn(II) and Co(II) disappeared and Pb(II) maintained the lead followed by Cu(II) and Cd(II). Thus, a 500 mg/L solution simultaneously loaded with Cd(II), Co(II), Cu(II), Pb(II), and Zn(II) has a lower selectivity for Co(II) and Zn(II) in terms of competition and occupation of available adsorption sites.

Comparing the prepared fly ash FAU zeolite with the reference sample shown in Fig. 9 a and b, within 10 minutes there was more than 99% removal of Pb(II) for both adsorbents at 200 mg/L. Cu(II) and Cd(II) removal were higher for the fly ash FAU zeolite than the reference zeolite. Just as in Fig. 8a, there is a wider separation in the adsorption trend curves between the first three preferentially adsorbed metals (Pb(II), Cu(II), and Cd(II)) and the least adsorbed metals - Co(II) and Zn(II). With the exception of Pb(II), the gap is fairly consistent with the other four metals in the case of the reference zeolite.

In assessing the efficiency at 200 mg/L and 90 mins duration for three different adsorbent loadings - 5, 10, and 15 g/L shown on Fig. 10, Pb(II) had an optimal removal at the lowest adsorbent loading of 5 g/L. The more noticeable changes in efficiency were Co(II) and Zn(II); doubling the initial adsorbent loading to 10 g/L led to more than a 50% increment in Co(II) removal and about a 30% increment in Zn(II). These results are logical since increasing the amount of adsorbents provides extra active sites for adsorption even in the most competitive and selective environment. Tripling the loading had no noticeable effect on Zn(II) since twice the initial loading provided sufficient adsorption active sites needed for its removal while Co(II) had about an 8% increment from the previous 50%. Table 3 shows the EDAX elemental analysis of prepared FAU zeolite, CFZ10-68, before and after adsorption for the three zeolite loadings used in Fig. 11. The semi-quantitative results show that all five metals were simultaneously removed from solutions. Similar levels of each metal were measured in filtered and dried zeolite samples independently of the zeolite loading used for adsorption. These levels decreased

with an increase in the zeolite loading from 5 g/L to 15 g/L due to the increased number of surface sites available for adsorption.

3.3.2 Kinetics and adsorption isotherm models

Though the data was tested on five kinetic models, only the best two (second-order and pseudo second-order) are presented on Table 4 for an initial concentration of 200 mg/L; pseudo second-order had the best fitting followed by second-order. The rate constants (k_2 , k_{PSO} , and k_{id}) are indicators of how fast adsorption occurs; the higher the value, the faster the adsorption. From the correlation factor, R^2 , the pseudo second-order kinetic model had the best fit for all five heavy metals; this is an indication of chemisorption in contrast to physisorption as the driving mechanism for the adsorption [1,41]. Equilibrium sorption capacity values, q_e , obtained from the pseudo second-order model fitting (Table 4) were comparable to the experimental values at 200 mg/L. The experimental values were 39.965 mg/g, 39.008 mg/g, 38.906 mg/g, 31.615 mg/g, and 16.400 mg/g for Pb(II), Cd(II), Cu(II), Zn(II), and Co(II) respectively. A model vs experimental q_e is therefore within a reasonable tolerance. The rate constant for the pseudo second-order model follows the trend: Pb(II) > Cd(II) > Cu(II) > Co(II) > Zn(II). Data fitting using the intraparticle diffusion model yielded a linear correlation (Table 4) with the trend in diffusion rate as Co(II) > Zn(II) > Pb(II) > Cd(II) > Cu(II). Adsorption for a concentration range of 100 mg/L to 500 mg/L on CFZ10-68 had the best fitting with the Langmuir adsorption isotherm and the isotherm parameters are shown on Table 5. The model/theoretical values were compared with the actual experimental values and the difference was within $\pm 2\%$ which is reasonable except in the case of Co(II) that gave an underestimation of the actual value. For instance, in applying the model to Cu(II), the theoretical q_{max} is 57.803 mg/g, while the actual experimental value obtained was 58.024 mg/g; well within the tolerance limit. The maximum amount of metals adsorbed on FAU zeolite prepared from coal fly ash had the trend Pb(II) > Cu(II) > Cd(II) > Zn(II) > Co(II). Table 6 shows the Langmuir parameters, q_{max} and K_L , for the reference material, ZRef-FAU with the trend in maximum adsorption amounts as follows: Pb(II) > Cd(II) > Cu(II) > Zn(II) > Co(II). In comparing the maximum amounts adsorbed, q_{max} , CFZ10-68 (Table 5 and Fig. 8a) and ZRef-FAU (Table 6 and Fig. 8b) had approximately

similar amounts for Cu(II), Pb(II), and Zn(II). There were differences in the amounts of Cd(II) and Co(II) adsorbed whereby the reference material adsorbed more of these metals.

The ionic radii of the unhydrated metals have a size trend of $\text{Pb(II)} > \text{Cu(II)} > \text{Zn(II)} > \text{Cd(II)}$ [47]; for the hydrated ions, the trend would be reversed since there is an inverse proportional relationship between the radii of unhydrated cations and hydrated cations [48]. This trend is true for the adsorption of the first two ions (Pb(II) and Cu(II)) but is not necessarily true for the others. Cd(II) has the possibility of 4 (tetrahedral) and 6 (octahedral) coordination; Co(II) has 4, 6, and 8, Cu(II) has 4 and 6, Pb(II) has 6 and 8, and Zn(II) has 4, 6, and 8 coordination. The hydrated ionic sizes with the coordination number could be responsible for the high selectivity of Pb(II) even at the maximum concentration and the poor ion exchange capability for Co(II) in the presence of competing hydrated metal ions.

A study by Visa et al. [1] for Cu(II) and Cd(II) found the maximum adsorption capacity of the binary system on zeolite from unmodified coal fly ash was 58.1 mg/L and 16.1 mg/L respectively. In another study by Visa [7] for the simultaneous adsorption of Cd(II), Ni(II), Cu(II), Zn(II), and Pb(II) on zeolites from coal fly ash, with NaP1 as the major composition, the maximum adsorption capacity was found to be 26.9 mg/L for Cd(II), 20.9 mg/L for Cu(II), 5.9 mg/L for Ni(II), 7.9 mg/L for Zn(II), and 88.3 mg/L for Pb(II). Cheng et al. [4] did a study for Cu(II), Ni(II), Pb(II), and Cd(II) simultaneous adsorption on Linde type F zeolite from coal fly ash gave adsorption capacity of 18.5 mg/L, 9.1 mg/L, 46.5 mg/L, and 21.6 respectively at room temperature. Wang et al. [49] compared the adsorption of a binary system of Cu(II) and Zn(II) on Linde type A zeolite and zeolite X from coal fly ash; they found LTA zeolites have a better maximum adsorption performance than zeolite X – maximum adsorption capacity of 82.7 mg/L for Cu(II) and 47.4 mg/L for Zn(II). Using montmorillonite, Gupta et al. [50] found the adsorption of Pb(II), Cd(II), and Ni(II) on that clay was 31.1 mg/L, 30.7, and 21.1 mg/L respectively. From the literature data, a combination of Cd(II)/Zn(II)/Ni(II)/Cu(II)/ that includes Pb(II) would always have a higher selectivity towards Pb(II) as confirmed by the study presented here. Our study showed a higher adsorption capacity for 5 simultaneous loading of Pb(II), Cu(II), Cd(II), Zn(II), and Co(II) of 109.9 mg/g, 57.8 mg/g, 53.5 mg/g, 36.8 mg/g, and 12.2 mg/g respectively.

CONCLUSIONS

Coal fly ash was used to prepare zeolites and, depending on the synthesis conditions, the products were mainly composed of FAU-type zeolites. The prepared FAU zeolite sample (CFZ10-68) with a BET surface area of 432 m²/g was tested via adsorption studies for optimal time, concentration effect, and adsorbent loading in a five metals simultaneous system. The results showed that in the presence of competing ions, FAU zeolite prepared from coal fly ash can simultaneously remove heavy metals in aqueous solution. The trend for removal efficacy and adsorption isotherm model fitting was Pb(II) > Cu(II) > Cd(II) > Zn(II) > Co(II). A pseudo second-order (PSO) rate equation had the best fit while the Langmuir model described the adsorption isotherm. The maximum quantity adsorbed, q_{max} , was Pb(II) at 109.9 mg/g while Co(II) had the lowest at 12.2 mg/g.

ACKNOWLEDGEMENT

The authors thank the Schlumberger Foundation for their financial support. I.V. Joseph thanks Bolade O. Agboola and Victoria F. Adams (American University of Nigeria) for the productive discussions on this research.

REFERENCES

- [1] M. Visa, P. Nicoleta, A. Chelaru, Zeolite Materials Obtained from Fly Ash Used for Removal of Heavy Metals and dye from Complex Wastewaters, (2017).
- [2] USEPA, Framework for Metals Risk Assessment, 2007. www.epa.gov/osa (accessed July 26, 2018).
- [3] S. Chowdhury, M.A.J. Mazumder, O. Al-Attas, T. Husain, Heavy metals in drinking water: Occurrences, implications, and future needs in developing countries, *Sci. Total Environ.* 569–570 (2016) 476–488. doi:10.1016/j.scitotenv.2016.06.166.
- [4] T. Cheng, C. Chen, R. Tang, C.H. Han, Y. Tian, Competitive adsorption of Cu, Ni, Pb, and Cd from aqueous solution onto fly ash-based linde F(K) Zeolite, Iran. *J. Chem. Chem. Eng.* 37 (2018) 61–72. http://www.ijcce.ac.ir/article_31971_e25cf575d60edbc02902f7aad53c6952.pdf (accessed August 12, 2019).
- [5] P.P. Prabhu, B. Prabhu, A Review on Removal of Heavy Metal Ions from Waste Water using Natural / Modified Bentonite, *A Rev. Remov. Heavy Met. Ions from Waste Water Using Nat. Modif. Bentonite* Prathiksha. 02021 (2018) 1–13. doi:doi.org/10.1051/mateconf/201814402021.

- [6] J. Iqra, M. Faryal, R. Uzaira, T. Noshaba, Preparation of zeolite from incinerator ash and its application for the remediation of selected inorganic pollutants: A greener approach, in: IOP Conf. Ser. Mater. Sci. Eng., 2014. doi:10.1088/1757-899X/60/1/012060.
- [7] M. Visa, Synthesis and characterization of new zeolite materials obtained from fly ash for heavy metals removal in advanced wastewater treatment, Powder Technol. (2016). doi:10.1016/j.powtec.2016.02.019.
- [8] F.P. Venable, Zinc in drinking water, American Chemical Society, Geneva, 1884. doi:10.1016/S0140-6736(01)93477-4.
- [9] H. Cho, D. Oh, K. Kim, A study on removal characteristics of heavy metals from aqueous solution by fly ash, J. Hazard. Mater. 127 (2005) 187–195. doi:10.1016/j.jhazmat.2005.07.019.
- [10] S. Yadla, V. Sridevi, M. Lakshmi, Adsorption performance of fly ash for the removal of lead, Int. J. Eng. 1 (2012) 1–7. www.ijert.org.
- [11] H.A. Hegazi, Removal of heavy metals from wastewater using agricultural and industrial wastes as adsorbents, HBRC J. (2013). doi:10.1016/j.hbrcj.2013.08.004.
- [12] G. Kühn, Chapter 1 - Source materials for zeolite synthesis, in: H. Robson, K.P.B.T.-V.S. of Z.M. Lillerud (Eds.), Elsevier Science, Amsterdam, 2001: pp. 19–20. doi:https://doi.org/10.1016/B978-044450703-7/50099-5.
- [13] W. Franus, Characterization of X-type zeolite prepared from coal fly ash, Polish J. Environ. Stud. 21 (2012) 337–343.
- [14] C. Belviso, State-of-the-art applications of fly ash from coal and biomass: A focus on zeolite synthesis processes and issues, Prog. Energy Combust. Sci. 65 (2018) 109–135. doi:10.1016/j.pecs.2017.10.004.
- [15] S. Mintova, Verified Syntheses of Zeolitic materials: Third Edition, 2016. http://www.iza-online.org/synthesis/Vs_3rdEd.pdf.
- [16] V. Berggaut, A. Singer, High capacity cation exchanger by hydrothermal zeolitization of coal fly ash, Appl. Clay Sci. 10 (1996) 369–378. doi:10.1016/0169-1317(95)00033-X.
- [17] L. Tosheva, A. Brockbank, B. Mihailova, J. Sutula, J. Ludwig, H. Potgieter, J. Verran, Micron- and nanosized FAU-type zeolites from fly ash for antibacterial applications, J. Mater. Chem. 22 (2012) 16897–16905. doi:10.1039/c2jm33180b.
- [18] Z.T. Yao, X.S. Ji, P.K. Sarker, J.H. Tang, L.Q. Ge, M.S. Xia, Y.Q. Xi, A comprehensive review on the applications of coal fly ash, Earth-Science Rev. 141 (2015) 105–121. doi:10.1016/j.earscirev.2014.11.016.

- [19] FHWA, Steel Slag - Material Description - User Guidelines for Waste and Byproduct Materials in Pavement Construction - FHWA-RD-97-148, FHWA-RD-97-148. (2016). <https://www.fhwa.dot.gov/publications/research/infrastructure/structures/97148/cfa51.cfm> (accessed September 7, 2018).
- [20] A. International, ASTM C 618: Standard Specification for Coal Fly Ash and Raw or Calcined Natural Pozzolan for Use in Concrete, Annu. B. ASTM Stand. 04 (2017) 5. doi:10.1520/C0618-17A.
- [21] H. Höller, U. Wirsching, Zeolites formation from fly ash, *Fortschritte Der Mineral.* 63 (1985) 21–43.
- [22] V. Komvokis, L.X.L. Tan, M. Clough, S.S. Pan, B. Yilmaz, Zeolites in Sustainable Chemistry, in: *Zeolite Sustain. Chemistry*, Springer, Berlin, Heidelberg, Berlin, 2016: pp. 271–297. doi:10.1007/978-3-662-47395-5_8.
- [23] S.M. Auerbach, K.A. Carrado, P.K. Dutta, *Handbook of Zeolite Science and Technology*, Taylor & Francis, 2003. doi:10.1016/S1351-4180(04)00164-3.
- [24] J. Weitkamp, Zeolites and catalysis, *Solid State Ionics.* 131 (2000) 175–188. doi:10.1016/S0167-2738(00)00632-9.
- [25] C.S. Cundy, P.A. Cox, The hydrothermal synthesis of zeolites: History and development from the earliest days to the present time, *Chem. Rev.* 103 (2003) 663–701. doi:10.1021/cr020060i.
- [26] M. Moshoeshoe, S. Nadiye-Tabbiruka, V. Obuseng, A Review of the Chemistry, Structure, Properties and Applications of Zeolites, *Am. J. Mater. Sci.* 7 (2017) 196–221. doi:10.5923/j.materials.20170705.12.
- [27] G.G. Hollman, G. Steenbruggen, M. Janssen-Jurkovičová, Two-step process for the synthesis of zeolites from coal fly ash, *Fuel.* 78 (1999) 1225–1230. doi:10.1016/S0016-2361(99)00030-7.
- [28] N. Murayama, H. Yamamoto, J. Shibata, Mechanism of zeolite synthesis from coal fly ash by alkali hydrothermal reaction, *Int. J. Miner. Process.* 64 (2002) 1–17. doi:10.1016/S0301-7516(01)00046-1.
- [29] X. Querol, N. Moreno, J.C. Umaa, A. Alastuey, E. Hernández, A. López-Soler, F. Plana, Synthesis of zeolites from coal fly ash: an overview, *Int. J. Coal Geol.* 50 (2002) 413–423. doi:10.1016/S0166-5162(02)00124-6.
- [30] S.S. Bukhari, J. Behin, H. Kazemian, S. Rohani, Conversion of coal fly ash to zeolite utilizing microwave and ultrasound energies: A review, *Fuel.* (2015). doi:10.1016/j.fuel.2014.09.077.
- [31] S.S. Bukhari, J. Behin, H. Kazemian, S. Rohani, Synthesis of zeolite NA-A using single mode

- microwave irradiation at atmospheric pressure: The effect of microwave power, *Can. J. Chem. Eng.* 93 (2015) 1081–1090. doi:10.1002/cjce.22194.
- [32] J.L.X. Hong, T. Maneerung, S.N. Koh, S. Kawi, C.-H. Wang, Conversion of Coal Fly Ash into Zeolite Materials: Synthesis and Characterizations, Process Design, and Its Cost-Benefit Analysis, *Ind. Eng. Chem. Res.* 56 (2017) 11565–11574. doi:10.1021/acs.iecr.7b02885.
- [33] X. Querol, N. Moreno, A. Alastuey, R. Juan, C. Ayora, A. Medinaceli, A. Valero, C. Productos, Synthesis of high ion exchange zeolites from coal fly ash, *Geol. Acta.* 1 (2007) 49–57. doi:10.1344/105.000000309.
- [34] B. Jha, D.N. Singh, Fly Ash Zeolites ,Advanced Structured Materials, 1st ed., Springer Singapore, Singapore, 2016. doi:10.1007/978-981-10-1404-8.
- [35] Z. Adamczyk, B. Białecka, Hydrothermal synthesis of zeolites from Polish coal fly ash, *Polish J. Environ. Stud.* (2005). doi:10.1179/1743676115Y.0000000063.
- [36] N. Shigemoto, H. Hayashi, K. Miyaura, Selective formation of Na-X zeolite from coal fly ash by fusion with sodium hydroxide prior to hydrothermal reaction, *J. Mater. Sci.* 28 (1993) 4781–4786. doi:10.1007/BF00414272.
- [37] S. Rayalu, S.U. Meshram, M.Z. Hasan, Highly crystalline faujasitic zeolites from flyash, *J. Hazard. Mater.* (2000). doi:10.1016/S0304-3894(00)00212-0.
- [38] C. Belviso, F. Cavalcante, A. Lettino, S. Fiore, Zeolite Synthesised from Fused Coal Fly Ash at Low Temperature Using Seawater for Crystallization, *Coal Combust. Gasif. Prod.* 1 (2009) 7–13. doi:10.4177/CCGP-D-09-00004.1.
- [39] W. Channabasavaraj, R. Reddy, A REVIEW ON CHARACTERIZATION AND APPLICATION OF FLY ASH ZEOLITES, 2017. <http://www.journalijdr.com> (accessed September 8, 2018).
- [40] V.P. Valtchev, K.N. Bozhilov, Transmission electron microscopy study of the formation of FAU-type zeolite at room temperature, *J. Phys. Chem. B.* (2004). doi:10.1021/jp048341c.
- [41] P.K. Sahoo, S. Tripathy, M.K. Panigrahi, S.M. Equeenuddin, Evaluation of the use of an alkali modified fly ash as a potential adsorbent for the removal of metals from acid mine drainage, *Appl. Water Sci.* 3 (2013) 567–576. doi:10.1007/s13201-013-0113-2.
- [42] H.K. Boparai, M. Joseph, D.M. O’Carroll, Kinetics and thermodynamics of cadmium ion removal by adsorption onto nano zerovalent iron particles, *J. Hazard. Mater.* 186 (2011) 458–465. doi:10.1016/j.jhazmat.2010.11.029.
- [43] J.-P. Simonin, J. Bouté, S. Whitaker, Intraparticle diffusion-adsorption model to describe

- liquid/solid adsorption kinetics, *Rev. Mex. Ing. Quim.* 15 (2016) 161–173. <https://hal.sorbonne-universite.fr/hal-01312850> (accessed July 30, 2019).
- [44] K. Sangita, B. Prasad, G. Udayabhanu, Synthesis of zeolite from waste fly ash by using different methods, *Asian J. Chem.* 28 (2016) 1435–1439. doi:10.14233/ajchem.2016.19682.
- [45] F. Rouquerol, J. Rouquerol, K. Sing, Adsorption by Powders and Porous Solids, *Adsorpt. by Powders Porous Solids.* (2014). doi:10.1016/c2010-0-66232-8.
- [46] K.S.W. Sing, R.T. Williams, Physisorption hysteresis loops and the characterization of nanoporous materials, *Adsorpt. Sci. Technol.* 22 (2004) 773–782. doi:10.1260/0263617053499032.
- [47] H.M. Selim, Competitive sorption and transport of heavy metals in soils and geological media, 2016. doi:10.2136/sssaj2013.0004br.
- [48] B. Tansel, J. Sager, T. Rector, J. Garland, R.F. Strayer, L. Levine, M. Roberts, M. Hummerick, J. Bauer, Significance of hydrated radius and hydration shells on ionic permeability during nanofiltration in dead end and cross flow modes, *Sep. Purif. Technol.* (2006). doi:10.1016/j.seppur.2005.12.020.
- [49] C. WANG, J. LI, X. SUN, L. WANG, X. SUN, Evaluation of zeolites synthesized from fly ash as potential adsorbents for wastewater containing heavy metals, *J. Environ. Sci.* 21 (2009) 127–136. doi:10.1016/S1001-0742(09)60022-X.
- [50] S. Sen Gupta, K.G. Bhattacharyya, Immobilization of Pb(II), Cd(II) and Ni(II) ions on kaolinite and montmorillonite surfaces from aqueous medium, *J. Environ. Manage.* 87 (2008) 46–58. doi:10.1016/j.jenvman.2007.01.048.

Table 1. Si/Al ratio and BET results of synthesized zeolites.

Sample	Si/Al	SA (m ² /g)	SA _{ext} (m ² /g)	V _{micro} (cm ³ /g)
CFZ4-24	2.50	83	49	0.017
CFZ4-48	2.53	151	66	0.044
CFZ4-68	2.48	183	63	0.058
CFZ4-72	2.45	205	78	0.065
CFZ10-24	2.46	322	78	0.126
CFZ10-48	2.56	389	81	0.148
CFZ10-68	2.51	432	76	0.172
CFZ10-72	2.54	397	78	0.164
ZRef - FAU	2.30	626	43	0.304

Table 2. Si/Al ratio and textural characteristics of CFZ-68 samples prepared with different water content.

Sample	Si/Al	SA (m ² /g)	SA _{ext} (m ² /g)	V _{micro} (cm ³ /g)
CZ4-68	2.48	183	63	0.058
CZ10-68	2.50	432	76	0.172
CZ15-68	2.66	465	88	0.194
CZ20-68	2.54	27	14	0.007

Table 3. EDAX elemental analysis (wt%) of CFZ10-68 before and after adsorption experiments at different zeolite loadings (g/L).

Element	CFZ10-68	5 g/L	10 g/L	15 g/L
Si	21.09	17.49	19.29	14.71
Al	17.28	14.84	17.03	12.24
Cu	-	1.99	1.50	1.00
Cd	-	1.71	1.19	0.76
Co	-	1.92	1.18	0.74
Pb	-	1.99	1.30	1.17
Zn	-	1.75	1.33	0.78

Table 4. Kinetic parameters for CFZ10-68

Metal	Second-order		Pseudo second-order		Intraparticle diffusion		
	k_2 (L.min/mg)	R^2	q_e (mg/g)	k_{PSO} (g.min/mg)	R^2	k_{id} (mg.min ^{0.5} /g)	R^2
Pb(II)	0.100	0.972	40.000	0.893	1.000	0.412	0.971
Cd(II)	0.002	0.967	40.323	0.007	1.000	0.408	0.972
Cu(II)	0.001	0.997	39.683	0.012	1.000	0.3823	0.921
Zn(II)	0.000	0.997	34.722	0.002	0.997	0.478	0.986
Co(II)	0.000	0.961	19.531	0.004	0.995	0.852	0.989

Table 5. Langmuir adsorption isotherm parameters for CFZ10-68

Metal	$q_{\max}(\text{mg/g})$	$K_L(\text{L/mg})$	R^2
Pb(II)	109.890	3.250	0.987
Cd(II)	53.476	1.222	0.999
Cu(II)	57.803	0.700	1.000
Zn(II)	36.765	0.324	0.979
Co(II)	12.240	0.075	0.974

Table 6. Langmuir adsorption isotherm parameters for ZRef - FAU

Metal	$q_{\max}(\text{mg/g})$	$K_L(\text{L/mg})$	R^2
Pb(II)	103.093	4.409	0.990
Cd(II)	74.074	0.408	0.993
Cu(II)	57.803	0.221	0.988
Zn(II)	42.017	0.381	0.991
Co(II)	30.211	0.092	0.996

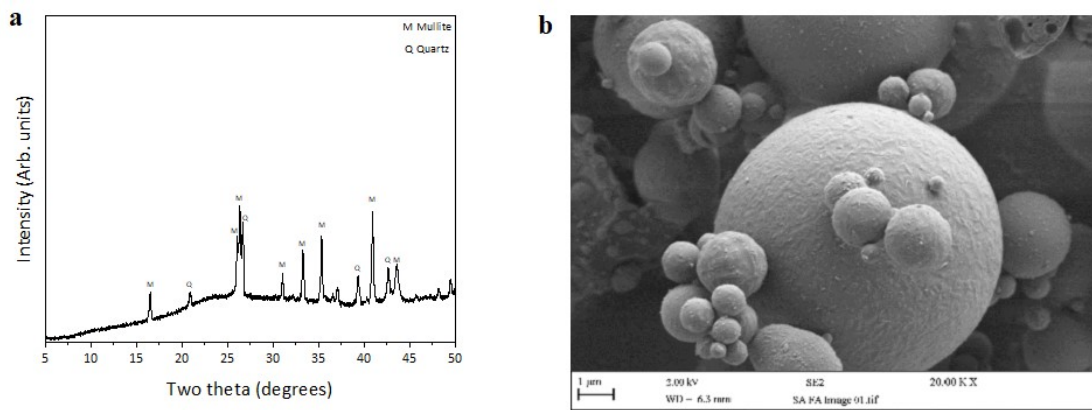


Fig. 1. (a) XRD pattern and (b) SEM image of untreated coal fly ash (CFA).

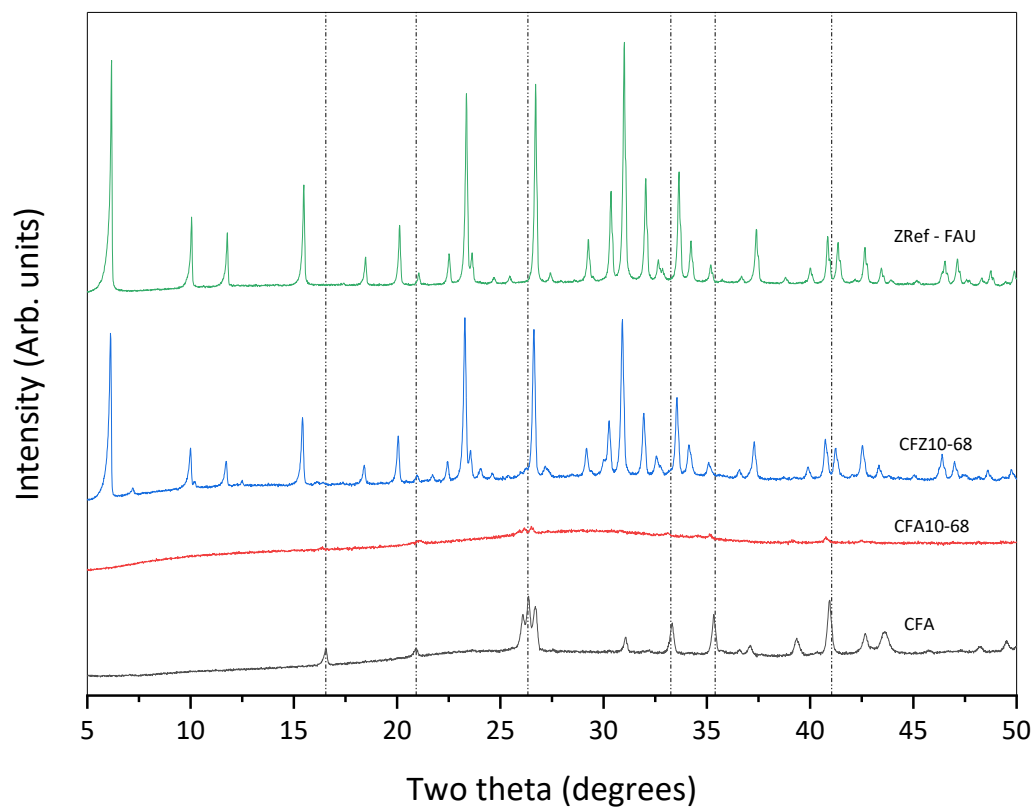


Fig. 2. XRD patterns showing the crystallography of CFA transformation to CFZ10-68 FAU zeolite for 68 h ageing. ZRef-FAU is the reference material.

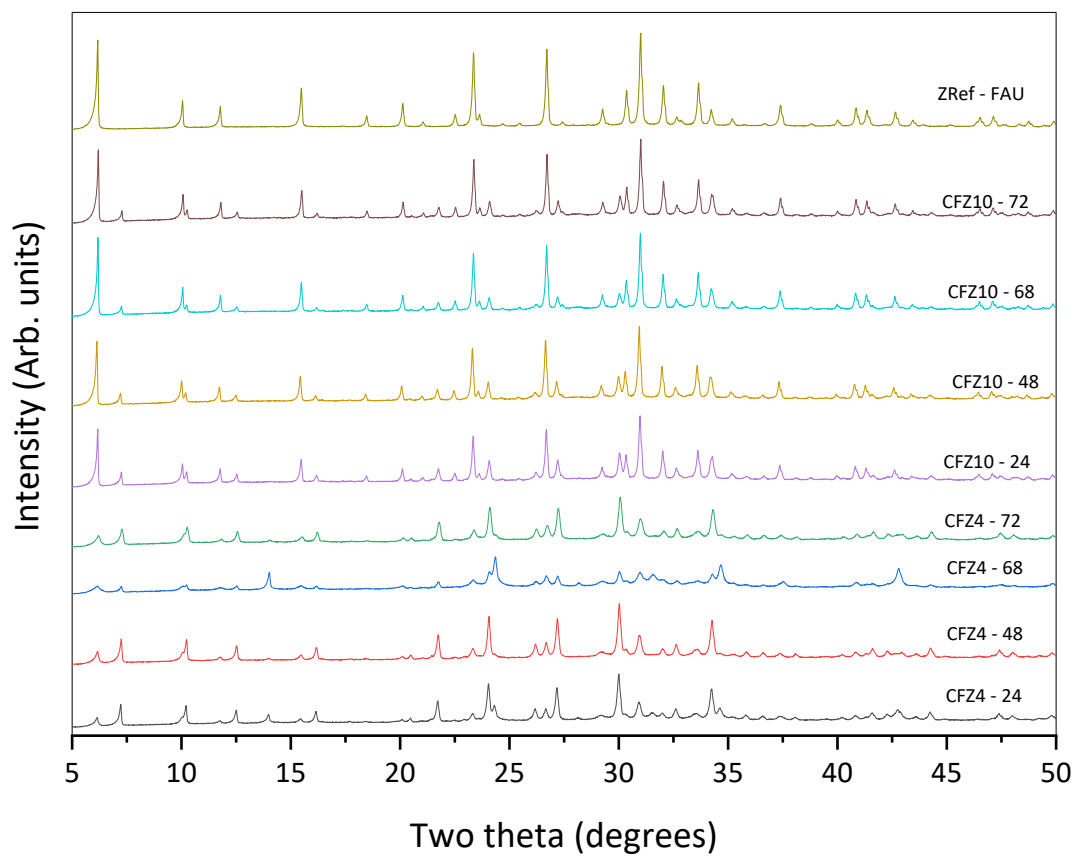


Fig. 3. XRD patterns for effects of ageing from 24 h to 72 h and water content from 1:4 to 1:10.

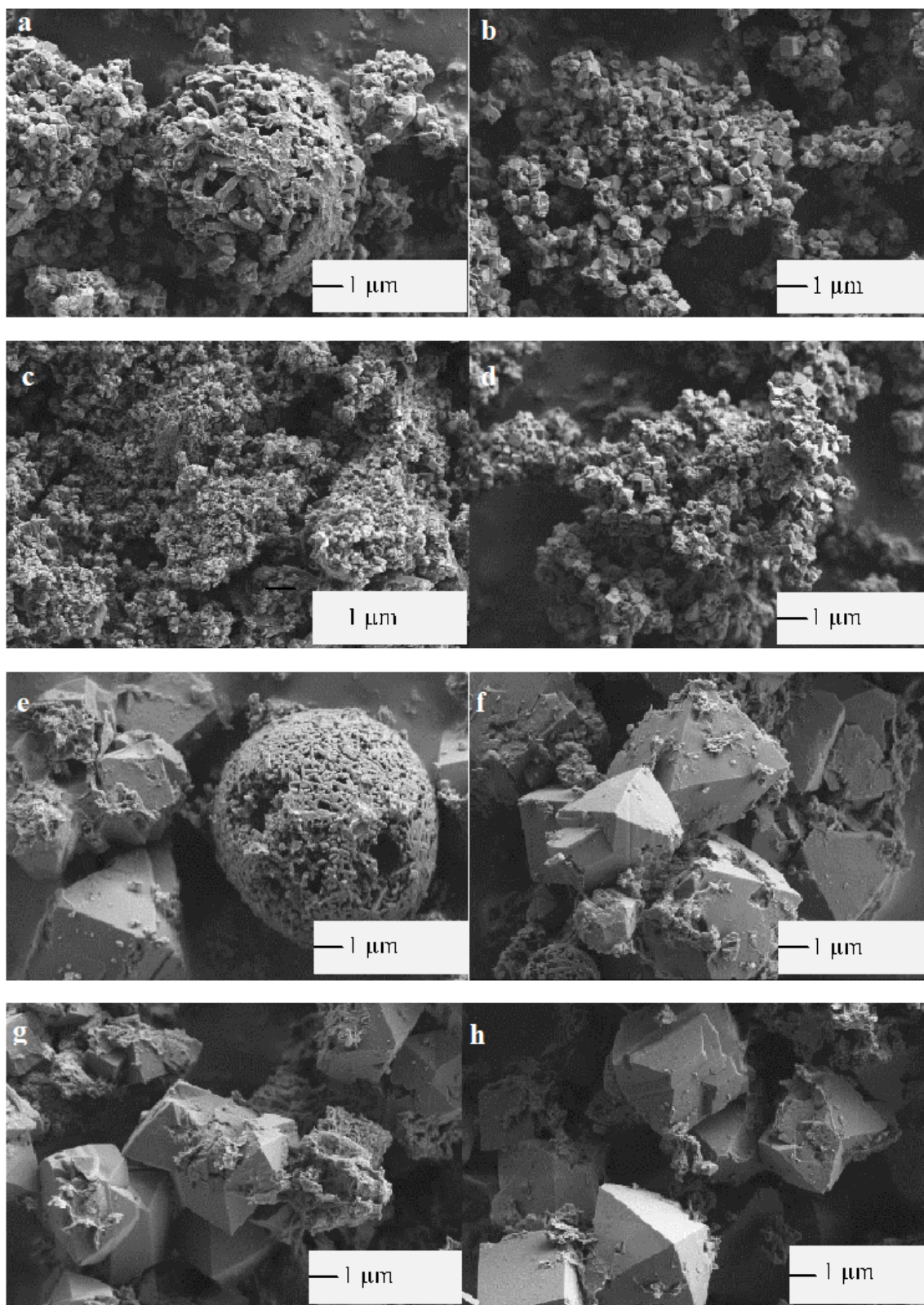


Fig. 4. SEM images of CFZ4-24, CFZ4-48, CFZ4-68, CFZ4-72 (a-d) and CFZ10-24, CFZ10-48, CFZ10-68, CFZ10-72 (e-h) water content.

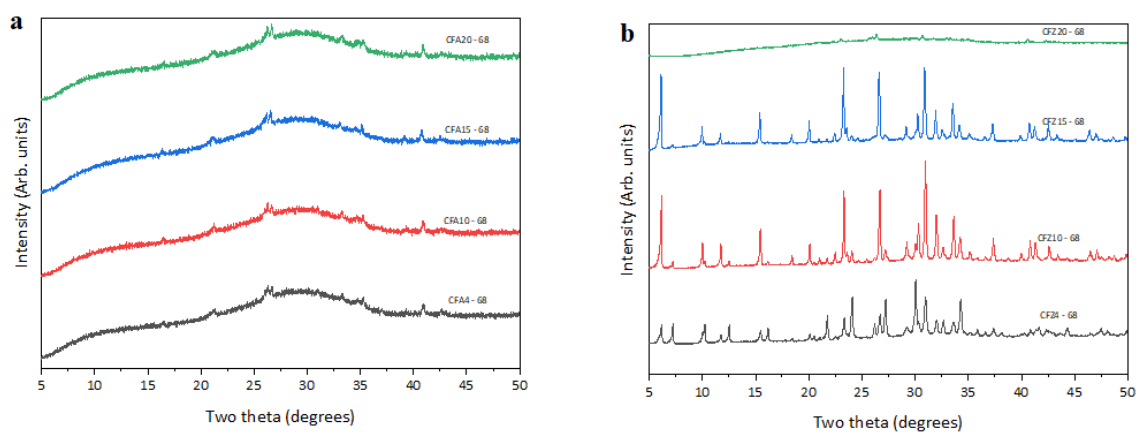


Fig. 5. XRD patterns of samples prepared with different water contents (a) pre hydrothermal CFA-68 and (b) zeolites CFZ4-68.

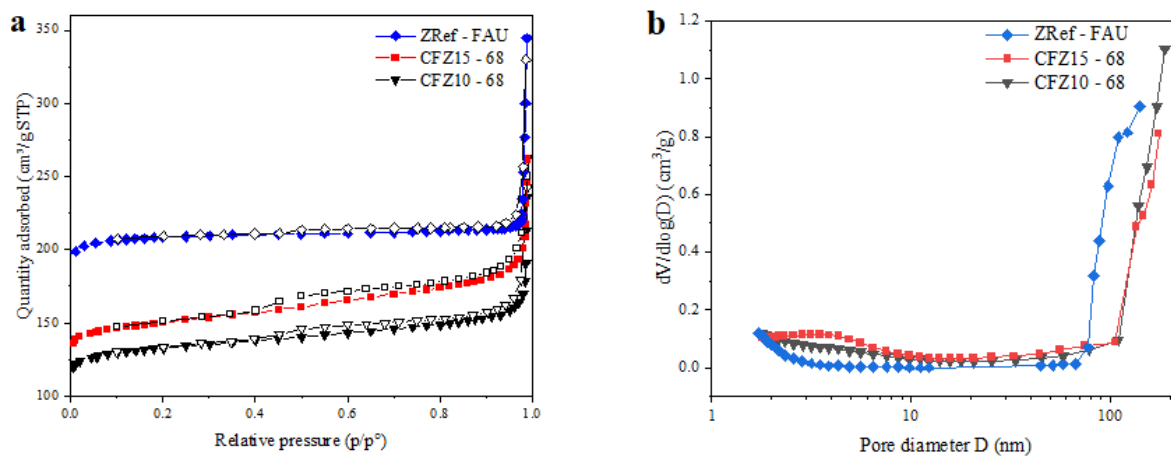


Fig. 6 (a) N₂ adsorption/desorption isotherms (close symbols, adsorption, open symbols, desorption) and (b) BJH Adsorption pore-size distributions of CFZ10-68, CFZ15-68, and ZRef-FAU samples.

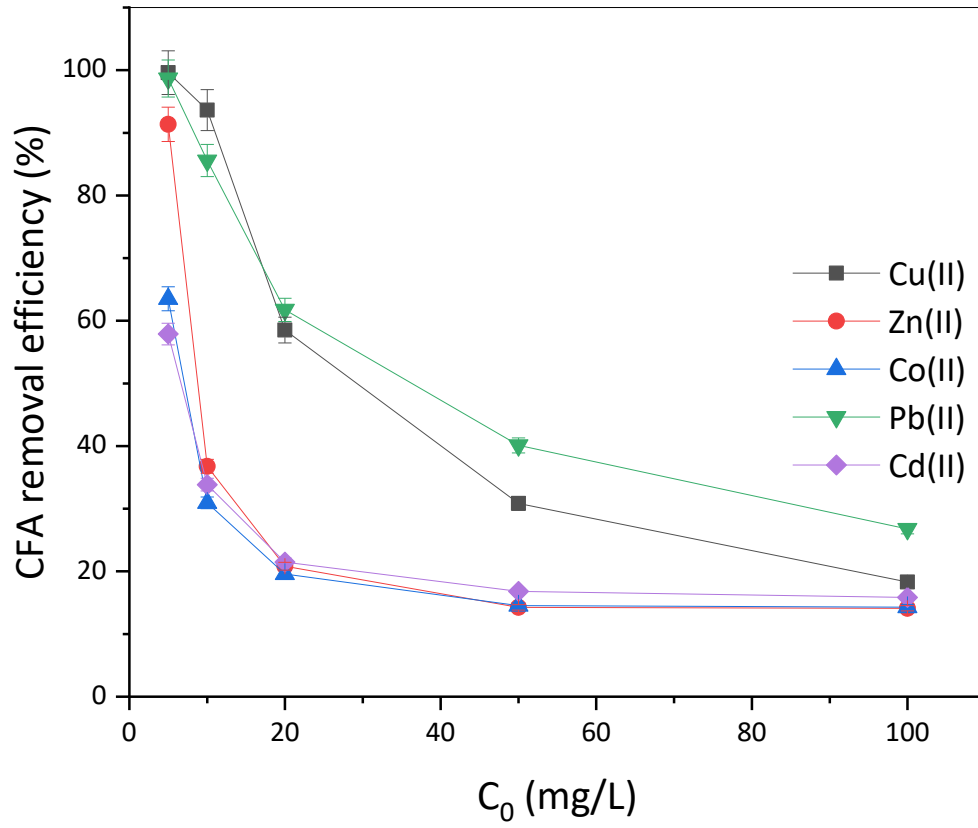


Fig. 7. Removal efficiency of untreated (raw) fly ash from 5 – 100 mg/L.

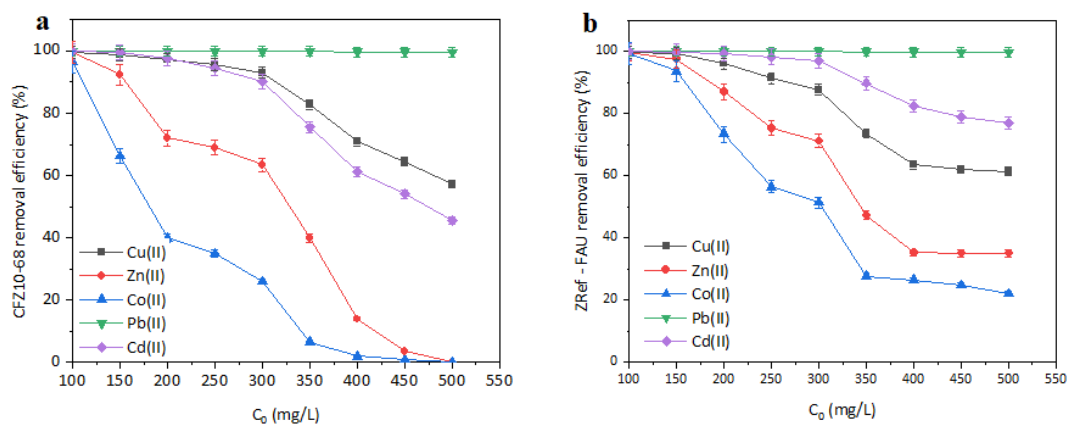


Fig. 8. Simultaneous removal of heavy metals for 100 – 500 mg/L at 90 min using (a) CZ10-68 and (b) ZRef-FAU.

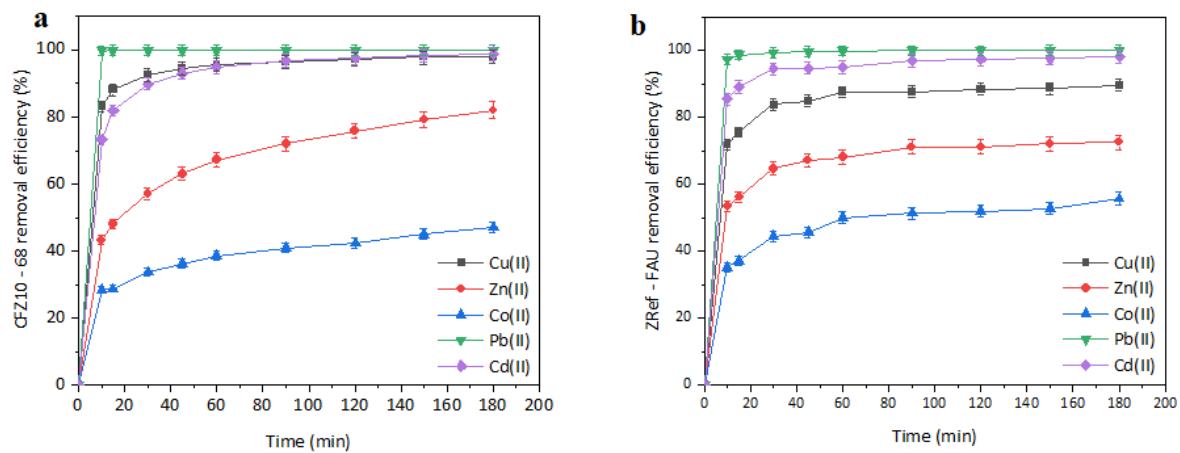


Fig. 9. Simultaneous removal of heavy metals for 0 – 180 min at 200 mg/L using (a) CZ10-68 and (b) ZRef-FAU.

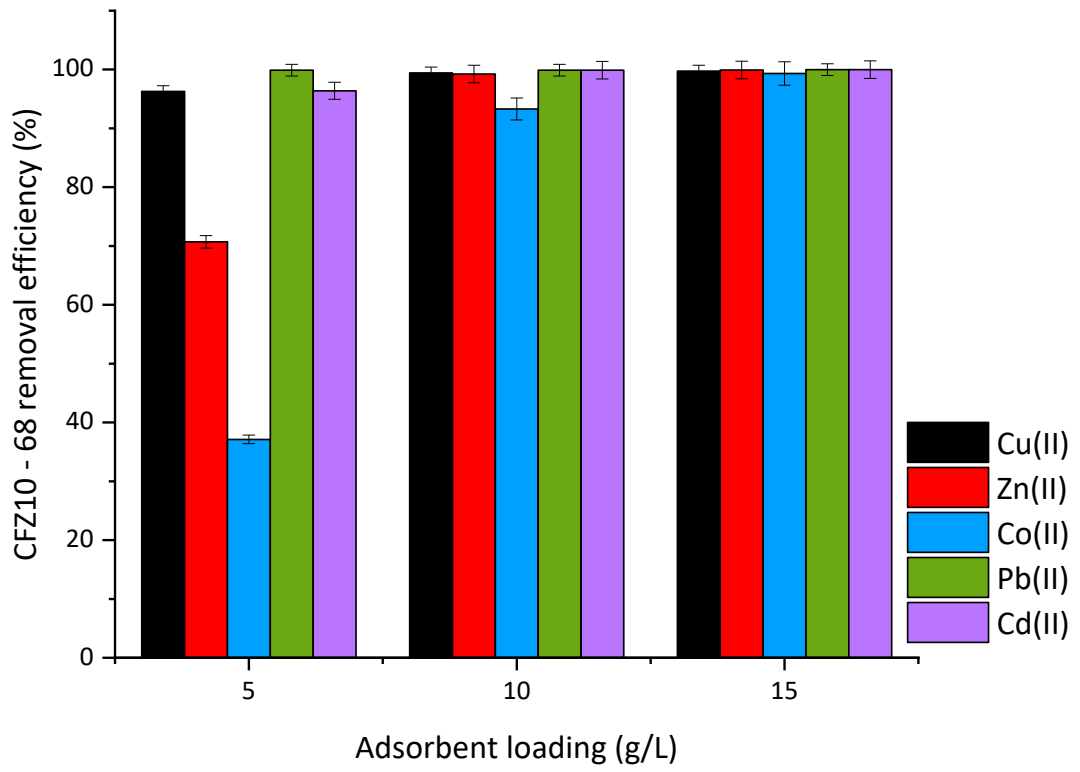


Fig. 10. CFZ10-68 loading variation for 200 mg/L at 90 min for heavy metals removal.